

## Impact of natural antioxidant (silybin) on the thermal stability of ultra high molecular weight polyethylene: a thermogravimetric study

Nidhi Khattar<sup>1</sup> · Jagriti<sup>1</sup> · Shagun Kainth<sup>2</sup> · Piyush Sharma<sup>2</sup> · Vishal Ahlawat<sup>3</sup> · Urmila Berar<sup>1</sup> · Pawan K. Diwan<sup>1</sup>

Received: 22 April 2024 / Accepted: 3 June 2024

Published online: 10 June 2024

© The Author(s) 2024 [OPEN](#)

### Abstract

The natural antioxidant (Silybin), with different concentrations, is introduced in Ultra High Molecular Weight Polyethylene (UHMWPE) and impact on thermal stability is observed. For this, thermograms are recorded at 5 °C/min heating rate in temperature region 50–600 °C through Thermogravimetric Analysis (TGA) technique. The model fitting (Coats and Redfern) kinetic approach is adopted to determine activation energy of each recorded thermograms to identify optimum silybin concentration. UHMWPE, with optimum silybin concentration, are further subjected to three other heating rates (10, 15 and 20 °C) in the same temperature region. By employing deconvolution (bi-Gaussian asymmetric function) approach, two iso-conversional kinetic models (Starink (SR) and Friedman (FR)) are utilized to obtain activation energies of the deconvoluted peaks. Further, the reaction mechanism involved in thermal decomposition, change in entropy ( $\Delta S^\ddagger$ ), change in enthalpy ( $\Delta H^\ddagger$ ) and change in Gibbs free energy ( $\Delta G^\ddagger$ ) are determined.

**Keywords** UHMWPE · Natural antioxidant · Silybin · Deconvolution · Thermodynamic parameters

## 1 Introduction

Ultra high molecular weight polyethylene (UHMWPE), an engineering polymer, is extensively utilized in numerous applications such as pipeline transportation, biological joints, bullet proof jacket, aerospace etc. [1–4]. These applications are possible only due to its excellent wear resistance, impact resistance and biocompatibility [5–9]. In spite of these excellent inherent properties, UHMWPE cannot be considered as potential candidate at higher temperature applications due to its low thermal stability [10–12]. For this, adequate thermal stabilizer can be introduced in UHMWPE matrix. Previous studies reveal that polyphenolic compounds are extensively used as thermal stabilizer in different polymeric materials as it helps in scavenging free radicals by transferring proton and itself gets stabilized due to resonance [13–15]. Further, natural polyphenolic thermal stabilizers like Gallic acid, dodecyl gallate, vitamin C, and vitamin E are also non-toxic in nature and have minimal adverse effects [16–20]. These stabilizers give proton from phenolic group to a macro-radical of polymer matrix and then converting to a much less reactive phenoxy radical by the delocalization of unpaired electron over the aromatic ring. Thermal stability of polymer is affectively improved when polyphenolic stabilizers are substituted at ortho and para positions [21].

Highly substituted polyphenolic compounds found in fruits and vegetables and categorized as flavonoids. These are made up of two benzene rings joined together by a three-carbon chain to form a closed pyran ring. Their structural

✉ Pawan K. Diwan, diwanpk74@gmail.com | <sup>1</sup>Department of Applied Science, UIET, Kurukshetra University, Kurukshetra 136 119, India. <sup>2</sup>Division of Research and Development, Lovely Professional University, Phagwara 144 411, India. <sup>3</sup>Department of Mechanical Engineering, UIET, Kurukshetra University, Kurukshetra 136 119, India.



designation is C6-C3-C6. Depending upon the substitution of pyran ring, flavonoids are classified as flavanones, flavones, flavonols, flavanonols, flavanols, and catechins. Silybin [3,5,7-trihydroxy-2-[3-(4-hydroxy-3-methoxyphenyl)-2-hydroxyethyl-2,3-dihydrobenzo[1,4]dioxin-6-yl]chroman-4-one] (Fig. 1) is a flavanone extracted from milk thistle. This flavanone follows three radical scavenging mechanisms to enhance thermal stability of the polymers [22]. These are single electron transfer (SET), hydrogen atom transfer (HAT) and radical adduct formation (RAF). Single electron transfer mechanism recognizes the capacity to donate/accept electrons by considering ionization energy and electron affinity; silybin is found to be electron donor species for stabilization of free radicals. As per HAT mechanism, free radicals ( $\cdot\text{OH}$ ,  $\text{RO}\cdot$  and  $\cdot\text{OOH}$ ) are stabilized to neutral species such as  $\text{H}_2\text{O}$ ,  $\text{ROH}$  and  $\text{H}_2\text{O}_2$ . Whereas, RAF mechanism stabilize peroxy free radical by forming stable adduct at different hydroxyl positions due to hydrogen bonding. In case of silybin, HAT is the most efficient mechanism for scavenging free radicals followed by RAF, in which intra-molecular hydrogen bonds are formed to stabilize the  $\cdot\text{OOH}$  radical [22–24].

In the present study, silybin is utilized as antioxidant to enhance the thermal stability of UHMWPE. Thermograms of UHMWPE, with varying concentration of silybin, at  $5\text{ }^\circ\text{C}/\text{min}$  heating rate are recorded through TGA/DTA technique. The activation energies adopting different reactions mechanism are determined by following model fitting kinetic method (Coats and Redfern) and identified the silybin's concentration where the thermal stability is maximum. Further, identified sample is subjected to four different heating rates and analyzed through deconvolution kinetic method with Gaussian asymmetric function. Afterwards, activation energy is determined by utilizing integral (Straink model) as well as differential (Friedman model) kinetic model. The reaction mechanism is identified through integral master plots and find out the pre-exponential factor. Finally, thermodynamic parameters, i.e., change in entropy ( $\Delta S^\ddagger$ ), change in enthalpy ( $\Delta H^\ddagger$ ) and change in Gibbs free energy ( $\Delta G^\ddagger$ ) are determined.

## 2 Material and methodology

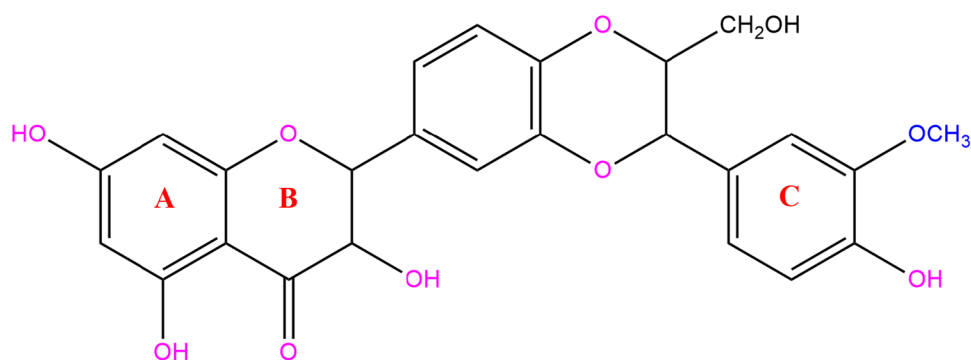
### 2.1 Material

UHMWPE (Ultra high molecular weight polyethylene) and Silybin powder are procured from Sigma Aldrich Co., USA. The molecular weight of UHMWPE is  $3 \times 10^6$ – $6 \times 10^6$  g/mol and density is 0.94 g/ml. The quoted percentage purity of Silybin is more than 98%, estimated through High Performance Liquid Chromatography (HPLC).

### 2.2 Sample preparation

1 wt % yellow colour silybin-ethanol solution is prepared by adding 0.05–0.5 g silybin, at an interval of 0.05 g, in ethanol. The prepared ethanolic solution is added in UHMWPE powder to form ten UHMWPE-Silybin samples of different concentrations (0.1 to 1.0 wt% with an interval of 0.1 wt %). Then, magnetic stirrer is used to homogenize the ethanolic-silybin solution in UHMWPE matrix. After that this homogenous mixture is dried in an oven at  $50\text{ }^\circ\text{C}$ . Further, these samples are stored overnight in desiccators, which contain anhydrous blue silica gel [25].

Fig. 1 Chemical structure of Silybin



## 2.3 Moulding of samples

Dried UHMWPE-Silybin samples are compacted in a designed mould under 5 MPa pressure at 25 °C temperature. Further, these samples are melted at 140 °C and compressed under the pressure of 15 MPa and then gradually cooled over 10 min of dwelling time. Finally, cylindrical shaped UHMWPE-Silybin samples of 12 mm diameter and 40 mm height are formed. These samples are cut with sharp blade to obtain 0.5 mm thickness of each sample.

## 2.4 Thermogravimetric analysis (TGA) technique

0.5 mm thickness samples (~0.5 mg weight) placed in alumina crucible one by one and subjected to thermogravimetric analysis (TGA) in an inert atmosphere of nitrogen gas at 100 ml/min flow rate. The mass loss is analysed as a function of temperature/time during thermal decomposition using a Hitachi STA 7200 TGA/DTA analyser. To ensure the accuracy of measurements, calibration of the system is performed. For temperature calibration, standard samples of indium (156.6 °C), tin (231.9 °C) and zinc (419.5 °C) with known melting points are used. These standard samples are placed in a platinum crucible one by one and heat-treated upto 200 °C for indium, 250 °C for tin and 500 °C for zinc at different heating rates (5, 10, 15, 20 °C/min) in a nitrogen atmosphere (100 ml/min). Through these measurements, the temperature of the Hitachi STA 7200 TGA/DTA analyzer is corrected. In the case of weight calibration, a standard weight of 20 mg (provided in the calibration kit of STA 7200) is used for weight correction. The TGA/DTA measured standard weight within a very small margin of error, typically within  $\pm 0.1\%$  of the known weight.

After calibration, ten samples are thermo-gravimetrically characterized at a single heating rate of 5 °C/min, in temperature region 50–600 °C. In addition, thermogravimetric analysis is also conducted at three other heating rates (10, 15 and 20 °C/min) on that sample having maximum thermal stability. These obtained thermograms are analyzed through ORIGIN software.

## 3 Theoretical approach

### 3.1 Kinetic theory

Polymeric materials undergo different thermal reactions at elevated temperature and as a result properties (mass loss or heat flow) of the material change. The obtained thermogravimetric (TG) data can be used for kinetic analyses, which will be helpful to provide information related to the thermal stability and service life of considered polymeric materials [26].

The rate of reaction involved in thermal decomposition of polymeric material can be described as:

$$\frac{d\alpha}{dt} = Ae^{\left(-\frac{E_a}{RT}\right)} f(\alpha) \quad (1)$$

$A$ ,  $E_a$ ,  $R$  and  $T$  are Arrhenius pre-exponential factor ( $\text{min}^{-1}$ ), activation energy ( $\text{kJmol}^{-1}$ ), gas constant ( $8.314 \text{ Jmol}^{-1} \text{ K}^{-1}$ ) and polymer temperature, respectively;  $f(\alpha)$  represents a differential form of degree of conversion ( $\alpha$ ), which can be derived through:

$$\alpha = \frac{m_i - m_t}{m_i - m_f} \quad (2)$$

$m_i$ ,  $m_t$  and  $m_f$  are initial mass, mass at time  $t$  and final mass of the sample, respectively.

By considering non-isothermal conditions, at linear heating rate, Eq. (1) can be rewritten as:

$$\frac{d\alpha}{dT} = \frac{A}{\beta} e^{\left(-\frac{E_a}{RT}\right)} f(\alpha) \quad (3)$$

$\beta = \frac{dT}{dt}$  is the linear heating rate ( $^{\circ}\text{C}/\text{min}$ ) and  $\frac{d\alpha}{dT}$  is rate of degree of conversion with respect to temperature.

When Eq. (3) is integrated, it results as:

$$g(\alpha) = \int_0^{\alpha} \frac{d\alpha}{f(\alpha)} = \frac{A}{\beta} \int_0^T e^{\left(-\frac{E_a}{RT}\right)} dT \quad (4)$$

$g(\alpha)$  represents an integral form of  $f(\alpha)$ .

Equation (3) and (4) serves as a base for developing different differential and integral kinetic models [27–33] using different approximations [34–37].

In the present study, the activation energy of UHMWPE-Silybin samples is determined by adopting different reaction mechanisms represented in Table 1 through the Coats and Redfern (CR) [27] kinetic model

$$\ln\left(\frac{-\ln(1-\alpha)}{T^2}\right) = \ln\left(\frac{AR}{\beta E_a}\right) + \ln\left(1 - \frac{2RT}{E_a}\right) - \frac{E_a}{RT} \quad (5)$$

### 3.2 Deconvolution method

This method is utilized to resolve the complexity involved in the second stage of thermal decomposition. In this study, the bi-Gaussian asymmetric function is applied to de-convolute the peaks.

$$y = \begin{cases} y_0 + He^{-0.5\left(\frac{x-x_c}{w_1}\right)^2} & \text{for } x < x_c \\ y_0 + He^{-0.5\left(\frac{x-x_c}{w_2}\right)^2} & \text{for } x \geq x_c \end{cases} \quad (6)$$

where  $y_0$  is baseline,  $H$  is the maximum height,  $x$  is the independent variable and  $x_c$  is the central value;  $w_1$  and  $w_2$  are the width of the left and right sides of the Gaussian peak.

**Table 1** Reaction mechanisms involved in thermal decomposition processes in solids

Reaction Mechanism	Symbol	$g()$
$n^{\text{th}}$ order reactions		
First order	F1	$-\ln(1-)$
Second order	F2	$-1 + (1-)^{-1}$
Third order	F3	$0.5[-1 + (1-)^{-2}]$
Diffusion mechanisms		
1D diffusion	D1	2
2D diffusion	D2	$\alpha + (1-\alpha)\ln(1-\alpha)$
3D diffusion (Jander equation)	D3	$\left[1 - (1-\alpha)^{1/3}\right]^2$
3D diffusion (Ginstling-Brounshtein equation)	D4	$1-(2/3)\alpha - (1-\alpha)^{2/3}$
Phase boundary reactions		
Cylinder symmetry	R2	$1 - (1-)^{1/2}$
Spherical symmetry	R3	$1 - (1-)^{1/3}$
Nucleation mechanisms		
Power law	P2	1/2
Power law	P3	1/3
Power law	P4	1/4
Power law	P2/3	3/2
Avrami-erofeev	A2	$[-\ln(1-)]^{1/2}$
Avrami-erofeev	A3	$[-\ln(1-)]^{1/3}$
Avrami-erofeev	A4	$[-\ln(1-)]^{1/4}$

**Fig. 2** Thermogravimetric (TG) curves of pure UHMWPE and stabilized UHMWPE with 0.1 wt% Silybin, at 5 °C/min heating rate

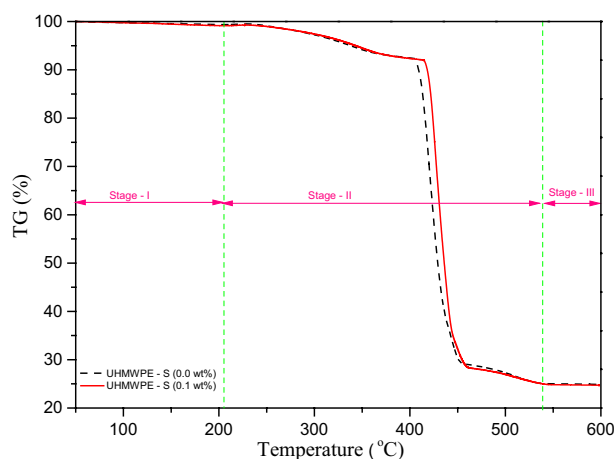
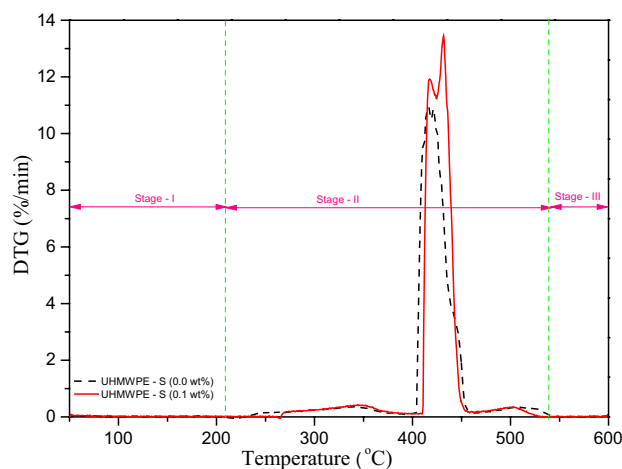


**Fig. 3** Derivative Thermogravimetric (DTG) curves of pure UHMWPE and stabilized UHMWPE with 0.1 wt% silybin, at 5 °C/min heating rate



### 3.3 Thermal kinetic parameters of stabilized UHMWPE-silybin samples

#### 3.3.1 Activation energy

After deconvolution, the activation energy of distinguished peaks is determined by employing the integral (Starink) model [32]:

$$\ln\left(\frac{\beta}{T^{1.92}}\right) = \ln\left(\frac{AR}{E_a}\right) + \ln\left(\frac{df(\alpha)}{d\alpha}\right) - 1.0008\frac{E_a}{RT} \quad (7)$$

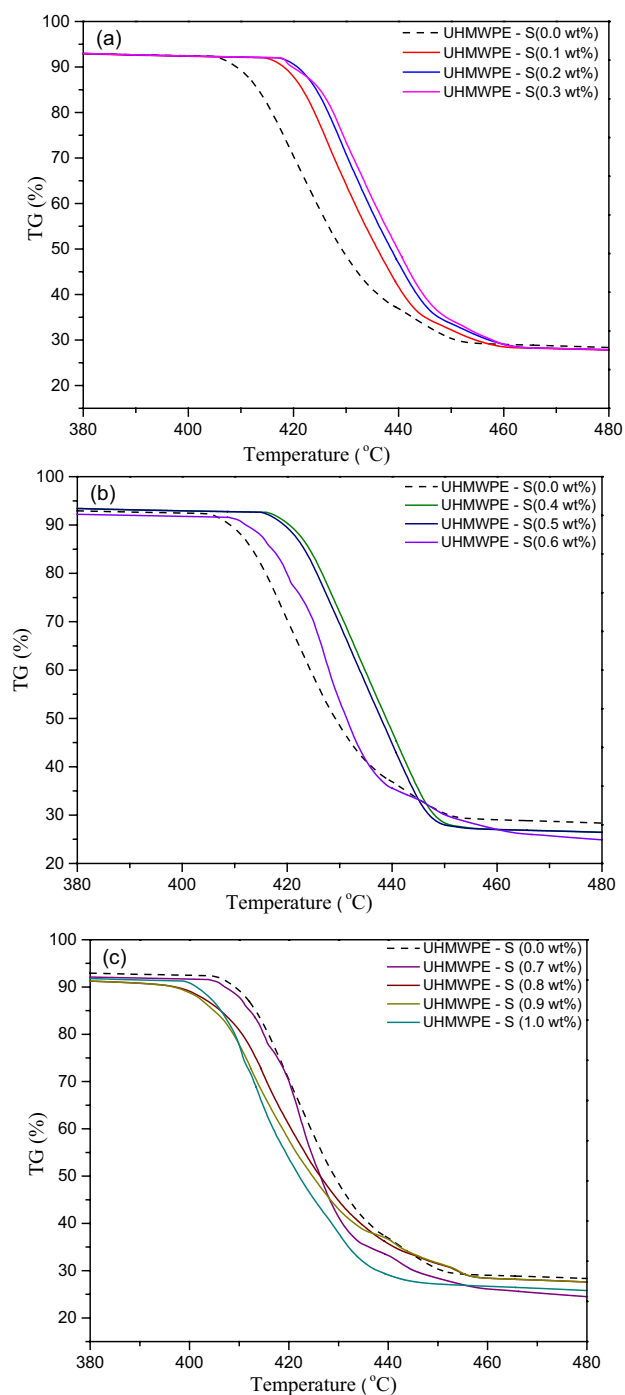
and differential (Friedman)[33]:

$$\ln\left(\beta\frac{d\alpha}{dT}\right) = \ln A + \ln f(\alpha) - \frac{E_a}{RT} \quad (8)$$

#### 3.3.2 Reaction mechanism

The activation energy obtained through Starink model is utilized to identify the exact reaction mechanism by adopting integral and master plots as:

**Fig. 4** TG/mass-loss curves of UHMWPE samples stabilized with different concentration of Silybin (S) **(a)** 0.0–0.3 wt%, **(b)** 0.0 and 0.3–0.6 wt% and **(c)** 0.0 and 0.7–1.0 wt%



$$g(\alpha) = \frac{AE_a}{\beta R} P(u) \tag{9}$$

$g(\alpha)$  is the integral function of conversion factor ( $\alpha$ ) and  $u = \frac{E_a}{RT}$ ;  $P(u)$  is the temperature integral and can be expressed as:

$$P(u) \approx \frac{\exp(-1.0008u - 0.312)}{u^{0.92}} \tag{10}$$

The reaction mechanism of stabilized UHMWPE is identified through the following relation:

**Table 2** Maximum decomposition temperature ( $T_{max}$ ) of Stage-II at different silybin concentrations

Silybin concentration (wt%)	$T_{max}$ (°C)
0.0	431
0.1	433
0.2	433
0.3	437
0.4	436
0.5	435
0.6	434
0.7	424
0.8	417
0.9	416
1.0	414

**Table 3** Activation energies (kJ/mol) obtained through the Coats and Redfern model, adopting different reaction mechanisms, at different silybin concentrations

Reaction mechanism	0.0	0.1	0.2	0.3	0.4	0.5	0.6	0.7	0.8	0.9	1.0
F1	462	498	513	549	546	527	522	507	439	427	415
F2	607	616	626	662	659	626	621	625	561	548	532
F3	789	743	762	792	789	745	740	769	722	692	687
D1	721	729	753	799	793	784	779	693	657	639	626
D2	781	789	804	843	842	828	723	745	717	792	683
D3	854	863	884	926	921	908	775	809	788	789	752
D4	802	814	836	889	884	846	741	767	741	721	707
R2	401	418	434	460	458	436	482	458	371	371	352
R3	413	422	439	479	472	469	495	474	389	390	363
P2	167	213	233	253	249	235	330	277	155	155	146
P3	102	115	131	159	156	148	290	230	99	98	91
P4	78	81	96	123	119	116	272	208	73	72	65
P2/3	538	593	608	621	618	611	563	554	494	490	466
A2	140	151	169	223	220	213	368	322	210	207	195
A3	101	113	127	158	150	134	315	260	94	92	89
A4	213	221	244	268	261	256	291	230	195	192	196

$$\frac{g(\alpha)}{g(0.5)} = \frac{P(u)}{P(0.5)} \quad (11)$$

The experimental ( $P(u)/P(0.5)$ ) points and theoretical ( $g(\alpha)/g(0.5)$ ) curves give the information of exact reaction mechanism involved in thermal decomposition of stabilized UHMWPE-Silybin sample.

### 3.3.3 Pre-exponential factor and thermodynamic parameters

By using identified reaction mechanism, pre-exponential factor ( $A$ ) is determined through Eq. (9).

Thermodynamic parameters such as change in entropy ( $\Delta S^\ddagger$ ), change in enthalpy ( $\Delta H^\ddagger$ ) and change in Gibbs free energy ( $\Delta G^\ddagger$ ) are determined through following mathematical relations [38–41]

**Fig. 5** Thermograms of UHMWPE with 0.3 wt% Silybin concentrations at four different heating rates (5, 10, 15 and 20 °C/min.)

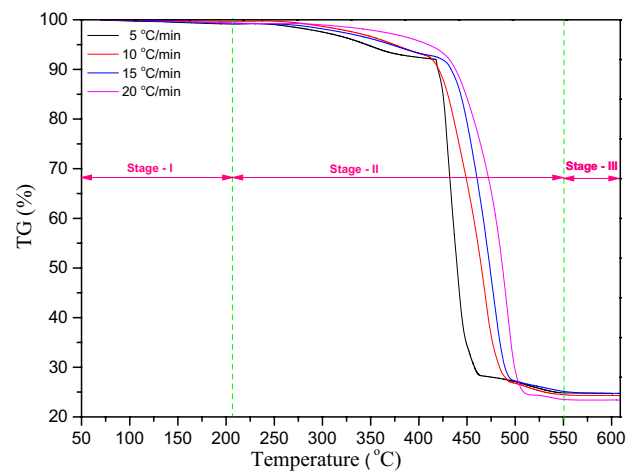
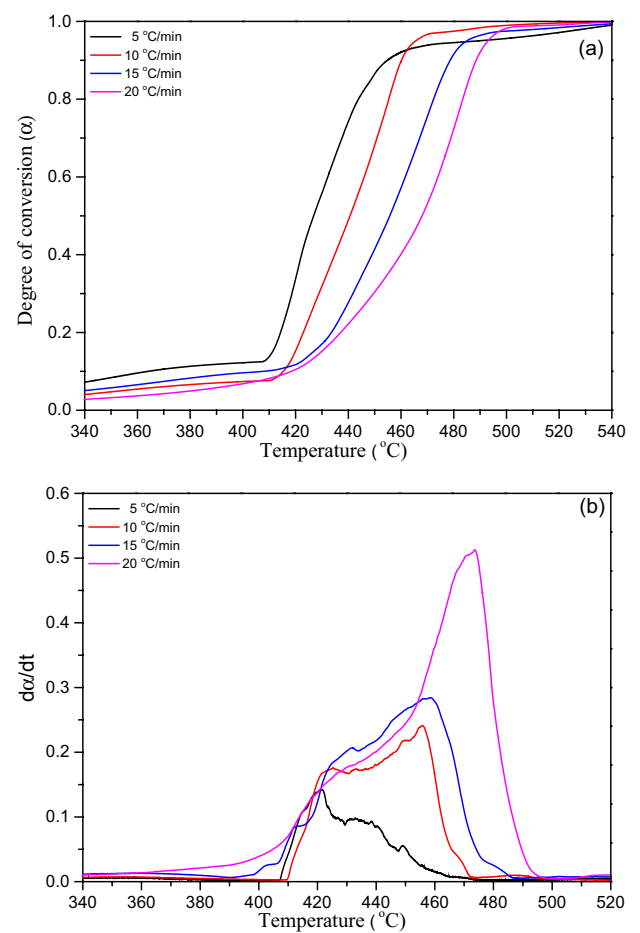


**Fig. 6** (a) Curves of degree of conversion ( $\alpha$ ) and (b) rate of degree of conversion ( $d\alpha/dt$ ) as a function of temperature, at four different heating rates (5, 10, 15 and 20 °C/min.)



$$\Delta S^\# = R \ln \left( \frac{A h}{e \chi k_B T_{max}} \right) \tag{12}$$

$$\Delta H^\# = E_a - RT_{max} \tag{13}$$

$$\Delta G^\# = \Delta H - T_{max} \Delta S \tag{14}$$



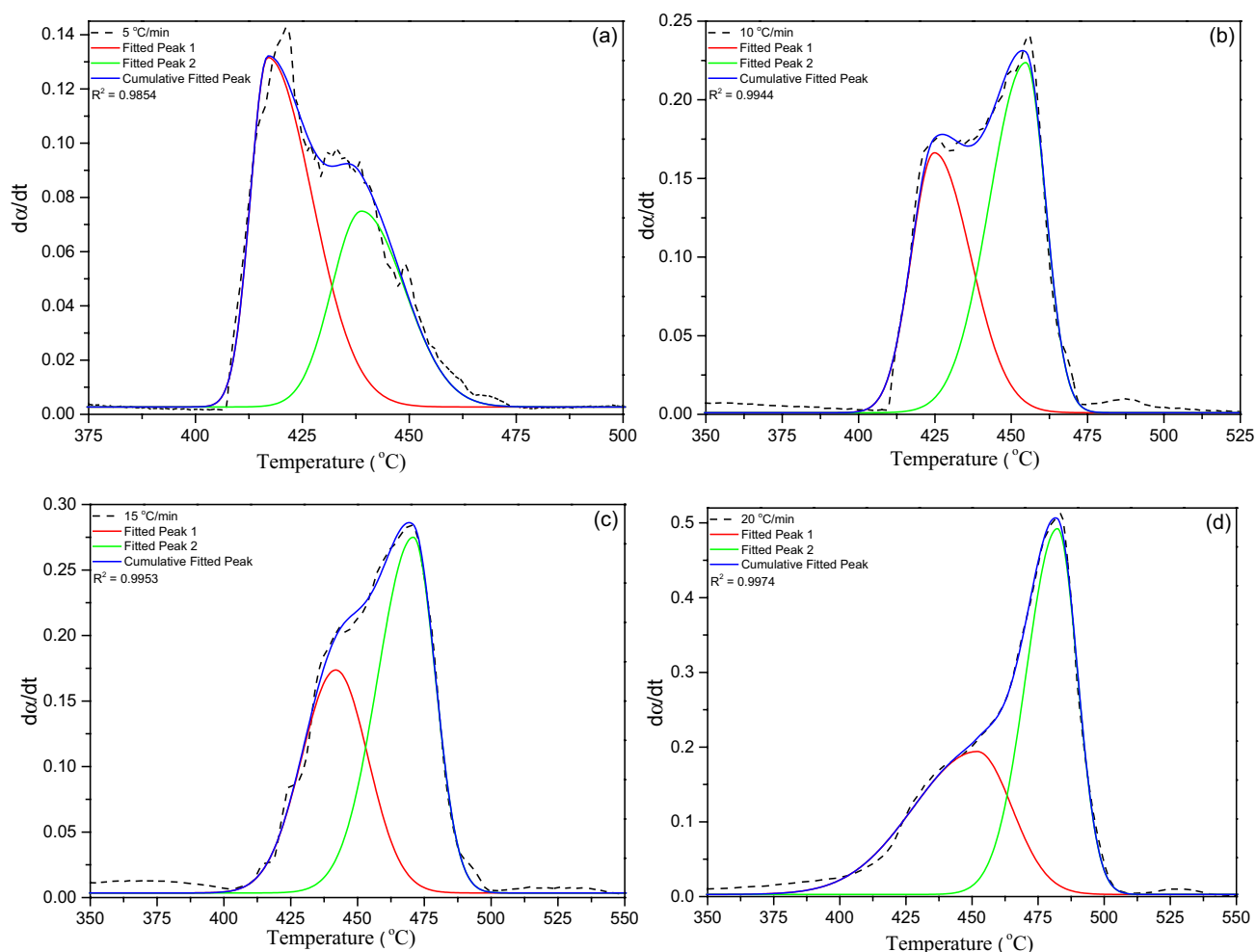


**Fig. 7** Deconvolution peaks of UHMWPE stabilized with Silybin (0.3 wt%) stabilized UHMWPE at (a) 5 °C/min, (b) 10 °C/min, (c) 15 °C/min and (d) 20 °C/min heating rates

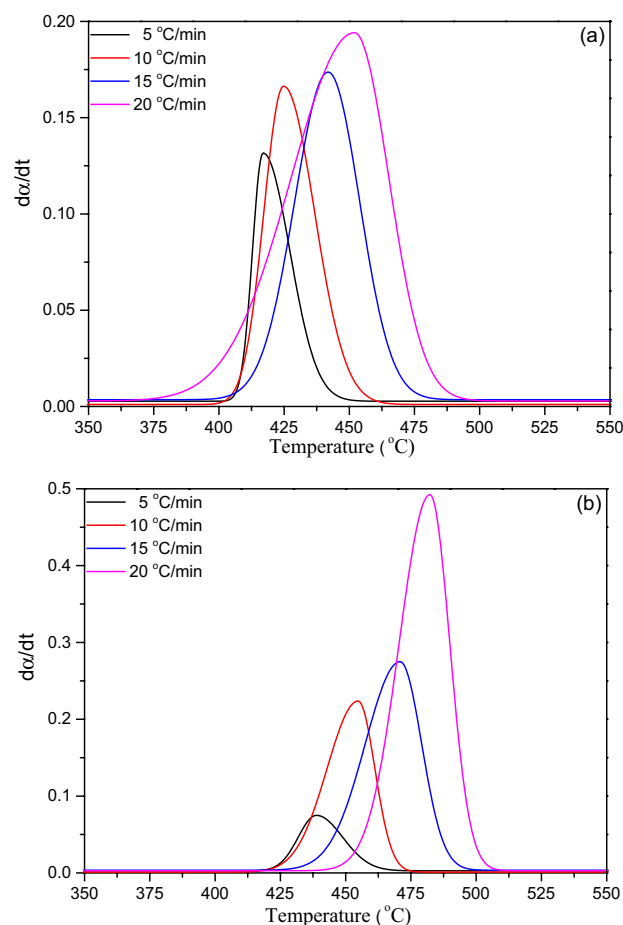
$A$  is a pre-exponential factor,  $h$  is Planck constant ( $6.626 \times 10^{-34} \text{ Js}^{-1}$ ),  $e$  is Neper number (2.7183),  $\chi$  is transition number which is equal to unity for monomolecular reaction,  $k_B$  is Boltzmann's constant ( $1.38 \times 10^{-23} \text{ Js}^{-1}$ ) and  $T_{max}$  is maximum decomposition temperature.

## 4 Result and discussion

### 4.1 Silybin as thermal stabilizer

Figure 2 presents thermograms of pure UHMWPE and UHMWPE blended with 0.1 wt% of silybin (S). Thermograms show three thermal decomposition stages and reveal positive impact of silybin on thermal stability of UHMWPE even at very low concentration (0.1 wt %). This enhancement, in thermal stability, is mainly due to the presence of phenolic group in the silybin. This phenolic group follows different possible pathways to halt the decomposition of UHMWPE. Firstly, by transferring its hydrogen atom to the free (peroxy, hydroxyl, alkoxide) radicals, which are formed during the oxidative decomposition of UHMWPE. In addition, silybin also gets stabilized by delocalization of phenoxide radical through resonance. Secondly, after the transfer hydrogen atoms, the phenoxide radical of silybin, also have the possibility to interact with other radical of UHMWPE to form radical adduct [23, 24, 42–44]. These adducts are more stable and less reactive for further decomposition. Figure 2 demonstrated an increase in maximum decomposition temperature, which leads to complicated thermal breakdown, as evident by the DTG curve (Fig. 3).

**Fig. 8** Rate of degree of conversion ( $d\alpha/dt$ ) as a function of temperature for (a) Peak 1 and (b) Peak 2, at four different heating rates (5, 10, 15 and 20 °C/min.)

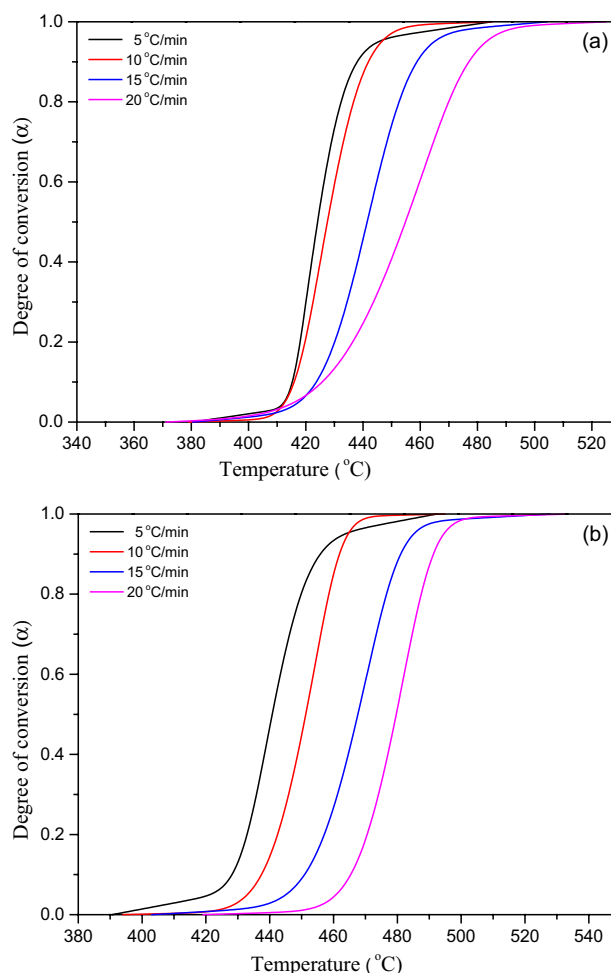


## 4.2 Effect of silybin concentration

As per Fig. 4a, thermal stability of UHMWPE increases with increase in concentration of silybin (S) up to 0.3 wt%. This may be due to increase in number of phenolic groups, which are helpful to scavenge free radicals, generated during thermal decomposition. Further, increase in concentration (0.4–0.6 wt %) in UHMWPE matrix decreases the thermal stability (Fig. 4b) due to poor dispersity of silybin resulting in formation of aggregates [45]. At higher concentration (0.7–1.0 wt%), thermal degradation (Fig. 4c) of UHMWPE starts due to the presence of large number of phenolic groups. Here, these groups itself react with oxygen present in UHMWPE matrix and as a results transformed into pro-oxidant by forming various oxidative products [46]. These figures reveal that maximum decomposition occurs in stage-II. Table 2 presents the maximum decomposition temperature ( $T_{max}$ ) as a function of silybin concentration. As per this discussion, silybin act as thermal stabilizer at lower concentration only and maximum thermal stability is at 0.3 wt% silybin.

In order to assure, thermal stability is maximum at 0.3 wt% only, activation energy at different silybin concentration for different reaction mechanisms are obtained through Coats and Redfern Kinetic model and presented in Table 3. From this, it is also observed that activation energy for considered reaction mechanism is maximum at 0.3 wt% as compared to other silybin concentrations.

**Fig. 9** Degree of conversion ( $\alpha$ ) as a function of temperature for (a) Peak 1 and (b) Peak 2, at four different heating rates (5, 10, 15 and 20 °C/min.)



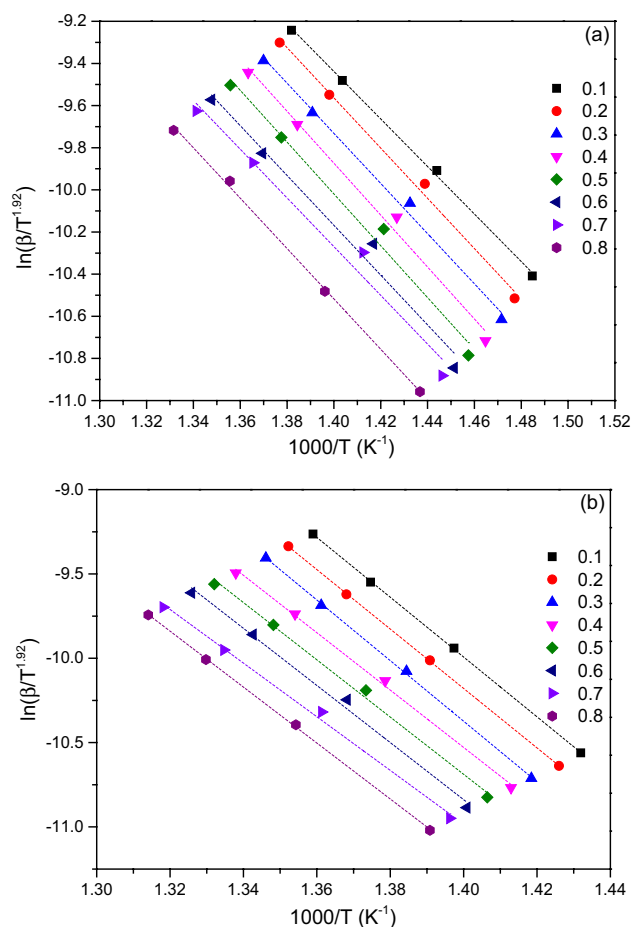
### 4.3 Thermal kinetic parameters of UHMWPE with 0.3 wt% silybin concentration

In order to explore different thermal kinetic parameters, thermograms of UHMWPE with 0.3 wt% silybin concentration at four different heating rates (5, 10, 15, 20 °C/min.) are obtained (Fig. 5). These thermograms (TG curves) show three thermal decomposition stages and Stage-II is highly active and complex. In addition, with an increase in heating rate, TG curves shifted toward higher temperatures side. Similar trends are also observed through Fig. 6a, b, presenting the curves of degree of conversion ( $\alpha$ ) and rate of degree of conversion ( $d\alpha/dt$ ) as a function of temperature. This may be due to thermal lag and consequently delay in radical participation in thermal decomposition. Further, Fig. 6b also presents the complexity involved in thermal decomposition of Stage-II.

#### 4.3.1 Deconvolution method

By adopting deconvolution method, complexities involved in thermal decomposition of Stage-II are resolved. Here, peaks (Fig. 6b) are deconvoluted using bi-Gaussian asymmetric function as per Eq. (6). Two peaks, one at 417 °C and the other at 439 °C are obtained at 5 °C/min heating rate (Fig. 7a). Similarly, two peaks at two distinct temperatures are also observed for other heating rates (Fig. 7b–d). First peak (Peak-1) and second peak (Peak-2) are shown as a

**Fig. 10** Linear fitted plots, at different degree of conversion ( $\alpha$ ) values, obtained through Starink model for (a) Peak 1 and (b) Peak 2



function of temperature in Figs.8a, b. Through these figs., degree of conversion ( $\alpha$ ) data is generated and presented in Fig. 9a, b as a function of temperature at different heating rates. These Figs. 8 and 9 reveal that peaks shifted towards higher temperature side with increase of heating rates, supporting the notion of thermal lagging.

#### 4.3.2 Estimation of activation energy

Activation energies are determined through linear fitted plots, at different degree of conversion ( $\alpha$ ) for Peak-1 and Peak-2 by adopting Starink (Fig. 10a and b) and Friedman (Fig. 11a and b) kinetic models. Starink model based activation energy first increases with increase of degree of conversion ( $\alpha$ ) and then decreases for both the peaks (Fig. 12). Here, activation energy of peak 1 is lower as compared to peak 2. On the other hand, in case of Friedman model, activation energy of peak 1 increases with increase of degree of conversion ( $\alpha$ ) while for peak 2 it decreases (Fig. 13). Friedman model based activation energy for peak 1 is higher than peak 2.

#### 4.3.3 Identification of reaction mechanism

By utilizing Starink model based activation energy, experimental points are generated through Eqs. (10) and (11) and presented as a function of degree of conversion ( $\alpha$ ) at four different heating rates (Figs. 14 and 15). Theoretical/master curves (adopting Eq. (9)) obtained through different reaction mechanisms and also incorporated in these Figures, for comparison. Through this, it is observed that Peak 1 and Peak 2 favours A4 and A3 (random nucleation) reaction mechanisms, respectively. These reaction mechanisms occur due to semi-crystalline nature of UHMWPEs resulting in restricting the mobility of free radicals, present in amorphous phase of UHMWPE [47].

**Fig. 11** Linear fitted plots, at different degree of conversion ( $\alpha$ ) values, obtained through Friedman model for (a) Peak 1 and (b) Peak 2

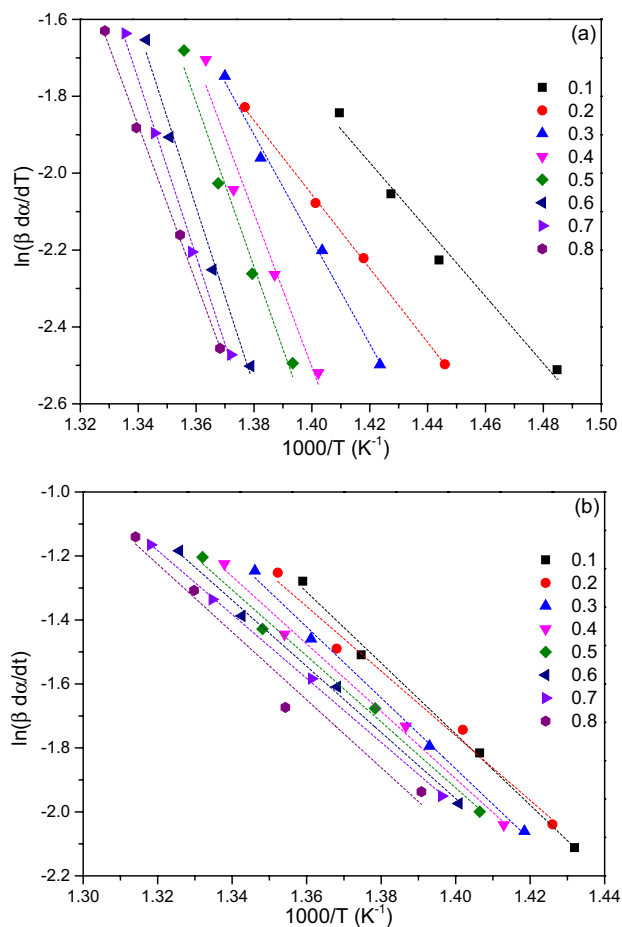


**Fig. 12** Variation of activation energy as a function of degree of conversion ( $\alpha$ ) of peak 1 and Peak 2, in case of Starink model

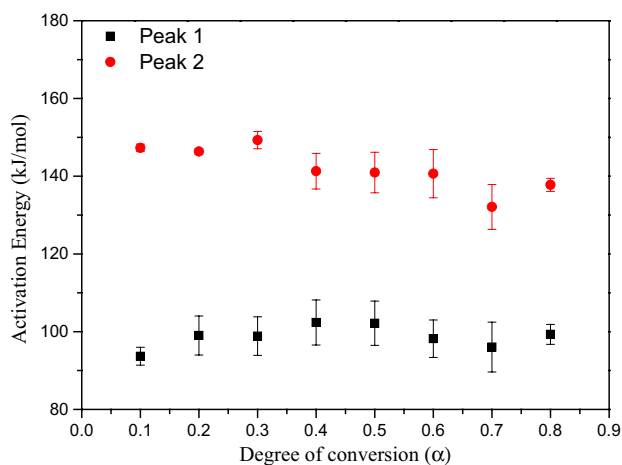


**Fig. 13** Variation of activation energy as a function of degree of conversion ( $\alpha$ ) of peak 1 and Peak 2, in case of Friedman model

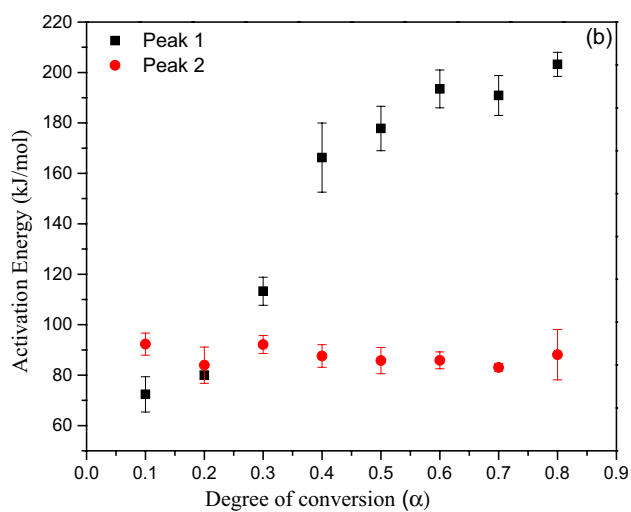


**Fig. 14** Comparison between experimental points and theoretical master's curves obtained for different nucleation mechanisms, for Peak 1

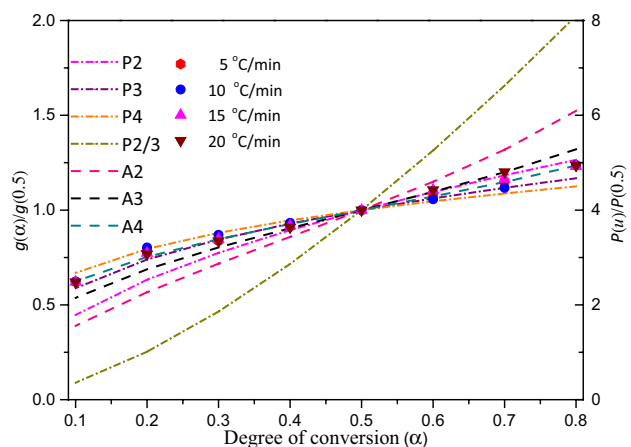


**Fig. 15** Comparison between experimental points and theoretical master's curves obtained for different nucleation mechanisms, for Peak 2

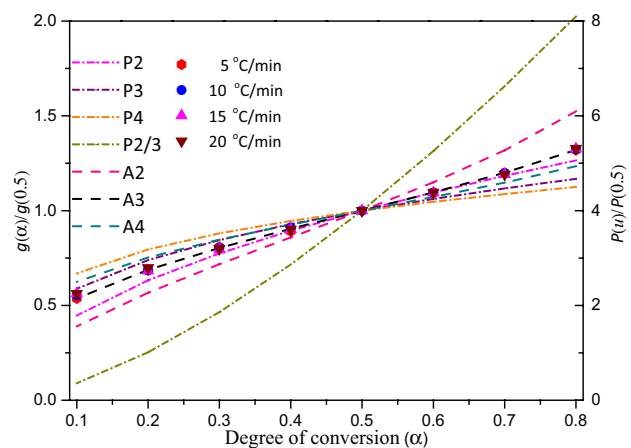
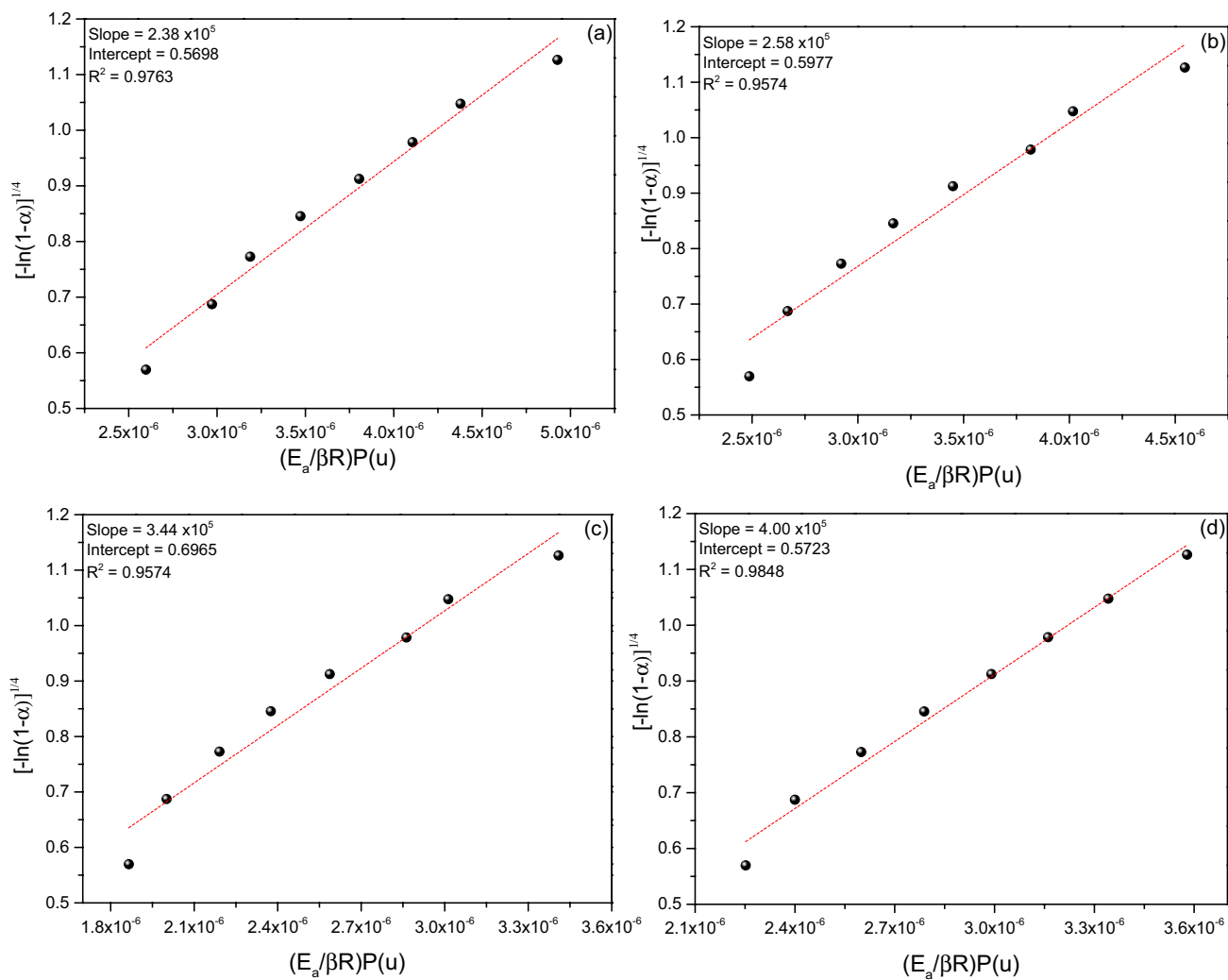


Fig.15



**Fig. 16** Linear fitted curves to obtain pre-exponential factors, at four different heating rates, for Peak 1

#### 4.3.4 Determination of pre-exponential factor and thermodynamic parameters

For pre-exponential factors ( $A$ ), Eq. (9) is rewritten by replacing  $g(\alpha)$  with A4 and A3 reaction mechanisms for Peak 1 and Peak 2, respectively.

$$[-\ln(1-\alpha)]^{1/4} = \frac{AE_a}{\beta R}P(u) \quad (15)$$

$$[-\ln(1-\alpha)]^{1/3} = \frac{AE_a}{\beta R}P(u) \quad (16)$$

By plotting linear fitted curves between  $[-\ln(1-\alpha)]^{1/4}$  and  $(E_a/\beta R)P(u)$  for Peak 1 (Fig. 16a–d) and  $[-\ln(1-\alpha)]^{1/3}$  and  $(E_a/\beta R)P(u)$  for Peak 2 (Fig. 17a–d), pre-exponential factors at different heating rate are determined and given in Tables 4 and 5.

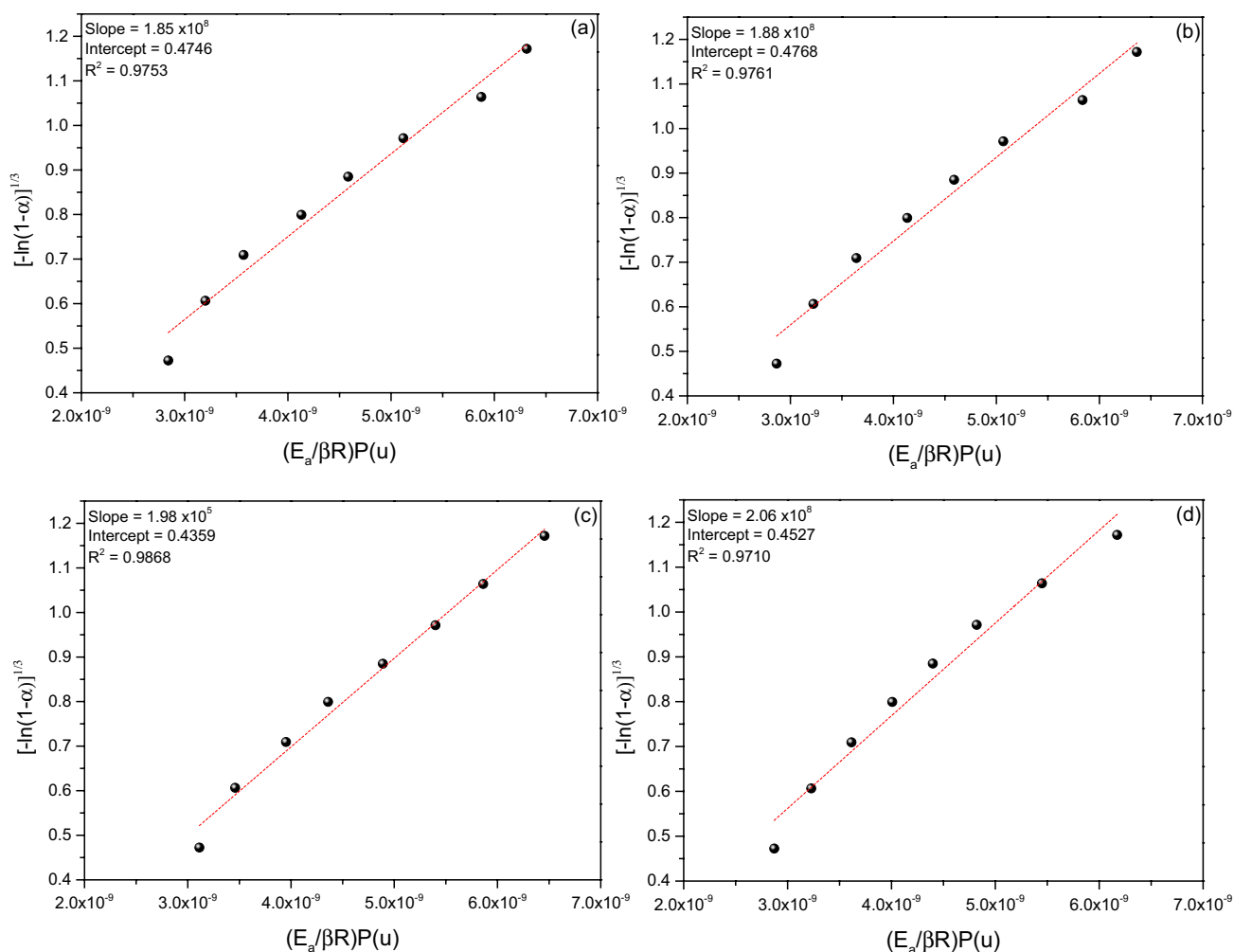


**Fig. 17** Linear fitted curves to obtain pre-exponential factors, at four different heating rates, for Peak 2

**Table 4** Pre-exponential factor and thermodynamic parameters of Peak 1 at different heating rates

Heating rate (°C/min)	$T_{max}$ (°C)	A (1/min)	$\Delta S$ (J/mol.K)	$\Delta H$ (kJ/mol)	$\Delta G$ (kJ/mol)
5	417	$2.38 \times 10^5$	-157.24	41.34	150.69
10	425	$2.58 \times 10^5$	-156.67	40.68	150.03
15	442	$3.44 \times 10^5$	-154.48	39.26	149.72
20	452	$4.00 \times 10^5$	-153.36	38.43	149.61

**Table 5** Pre-exponential factor and thermodynamic parameters of Peak 2 at different heating rates

Heating rate (°C/min)	$T_{max}$ (°C)	A (1/min)	$\Delta S$ (J/mol.K)	$\Delta H$ (kJ/mol)	$\Delta G$ (kJ/mol)
5	439	$1.85 \times 10^8$	-102.15	82.68	157.11
10	454	$1.88 \times 10^8$	-102.24	81.35	155.78
15	471	$1.98 \times 10^8$	-101.96	80.02	155.87
20	483	$2.06 \times 10^8$	-101.77	79.02	155.96



By utilizing pre-exponential factors ( $A$ ) and maximum decomposition temperatures ( $T_{max}$ ) in different mathematical relations (Eqs. (12)–(14)), change in entropy ( $\Delta S^\ddagger$ ), change in enthalpy ( $\Delta H^\ddagger$ ) and change in Gibbs free energy ( $\Delta G$ ) are determined (Tables 4 and 5) and observed negative values of  $\Delta G^\ddagger$  and positive values of  $\Delta H^\ddagger$  and  $\Delta G^\ddagger$  for both the peaks at different heating rates. These observations reveal that thermal decomposition, of UHMWPE blended with 0.3 wt % of natural antioxidant (silybin), is unfavourable.

## 5 Conclusions

Decomposition stages are unaffected by the silybin's blending into UHMWPE matrix, however, temperature regions of these stages are different at different silybin's concentrations. Silybin acts as a natural antioxidant at low concentrations (up to 0.6 wt%) and work as pro-oxidant at higher concentrations (0.7–1.0 wt%). The maximum thermal stability of UHMWPE is at 0.3 wt% Silybin. The complexity involved in Stage-II is resolved through deconvolution (bi-Gaussian distribution function) method. UHMWPE plus silybin is characterized by a non-spontaneous, endergonic random nucleation reaction mechanism, during thermal decomposition. The outcome of the study opens up new possibilities to utilize UHMWPE for higher temperature applications.

**Author contributions** Nidhi Khattar: Data curation, Methodology, Software. Jagriti: Writing—review & editing. Shagun Kainth: Writing—review & editing. Vishal Ahlawat: Writing-review & editing. Piyush Sharma: Writing—review & editing. Urmila Berar: Writing—review & editing. P.K. Diwan: Supervision, Validation, Writing—review & editing.

**Data availability** Data will be made available on request.

## Declarations

**Competing interests** The authors declare no competing interests.

**Open Access** This article is licensed under a Creative Commons Attribution 4.0 International License, which permits use, sharing, adaptation, distribution and reproduction in any medium or format, as long as you give appropriate credit to the original author(s) and the source, provide a link to the Creative Commons licence, and indicate if changes were made. The images or other third party material in this article are included in the article's Creative Commons licence, unless indicated otherwise in a credit line to the material. If material is not included in the article's Creative Commons licence and your intended use is not permitted by statutory regulation or exceeds the permitted use, you will need to obtain permission directly from the copyright holder. To view a copy of this licence, visit <http://creativecommons.org/licenses/by/4.0/>.

## References

1. Shammazov I, Karyakina E. The LNG flow simulation in stationary conditions through a pipeline with various types of insulating coating. *Fluids*. 2023;8(1–18):68.
2. Piska M, Urbancova K. Advanced machining of joint implant UHMWPE inserts. *Mach*. 2022;10(1–19):1008.
3. Zhimin Y, Xincong Z, Hongling Q, Wanying N, Hao W, Kai L, Yumin T. Study on tribological and vibration performance of a new UHMWPE/graphite/NBR water lubricated bearing material. *Wear*. 2015;332–333:872–8.
4. Chu Y, Chen X, Tian L. Modifying friction between ultra-high molecular weight polyethylene (UHMWPE) yarns with plasma enhanced chemical vapour deposition (PCVD). *Appl Surf Sci*. 2017;406:77–83.
5. Plumlee K, Schwartz CJ. Improved wear resistance of orthopaedic UHMWPE by reinforcement with zirconium particles. *Wear*. 2009;267:710–7.
6. Wang JH, Guo Y, Su YX, Xu XY, Duan TT, Wang LL, Yan SQ, Ruan GC, Xin PX, Wang L, Li N. New trends in ballistic UHMWPE UD fabric. *J Phys Conf Ser*. 2023;2460(1–7):012105.
7. Kadhim TR, Oleiwi JK, Hamad QA. Improving the Biological properties of UHMWPE biocomposite for orthopedic applications. *Int J Biomater*. 2023;2023:1–9.
8. Bozkaya O. chemical characterization of ultra high molecular weight polyethylene based tibial inserts after ethylene oxide sterilization. *Koc J Sci Engin*. 2023;6:51–60.
9. Turicek J, Ratts N, Kaltchev M, Masoud N. Surface treatment of ultra-high molecular weight polyethylene (UHMWPE) by cold atmospheric plasma (CAP) for biocompatibility enhancement. *Appl Sci*. 2021;11(1–12):1703.
10. Sui Y, Qiu Z, Liu Y, Li J, Cui Y, Wei P, Cong C, Meng X, Zhou Q. Ultra-high molecular weight polyethylene (UHMWPE)/high-density polyethylene (HDPE) blends with outstanding mechanical properties, wear resistance, and processability. *J Polym Res*. 2023;30(1–10):222.

11. Zaharescu T, Nicula N, Răpă M, Iordoc M, Tsakiris V, Marinescu VE. Structural insights into LDPE/UHMWPE blends processed by  $\gamma$ -Irradiation. *Polym.* 2023;15(1–24):696.
12. Guo Y, Cao C, Cheng H, Chen Q, Huang B, Luo F, Qian Q. Thermal performances of UHMWPE/BN composites obtained from different blending methods. *Adv Polym Technol.* 2019;2019:1–11.
13. Gaikwad KK, Deshmukh RK, Lee YS. Natural phenolic compound coated oxygen scavenging active polyolefin film for preserving quality of fish cake. *Biomass Convers Biorefin.* 2022;19:1–10.
14. Li X, Zhang J, Liu C, Mu W, Kong Z, Li Y, Wang Z, Yu Q, Cheng G, Chen L. Effects of pine needle extracts on the degradation of LLDPE. *Polym.* 2023;15(1–10):32.
15. Mateescu C, Zaharescu T, Mariş M. Chemiluminescence study on the radiochemical stability of polypropylene modified with microalgal extracts. *Radiat Phys Chem.* 2021;183(1–6):109401.
16. Moazzen A, Öztinen N, Ak-Sakalli E, Koşar M. Structure-antiradical activity relationships of 25 natural antioxidant phenolic compounds from different classes. *Heliyon.* 2022;8(1–11): e10467.
17. Shen J, Gao G, Liu X, Fu J. Natural polyphenols enhance stability of crosslinked UHMWPE for joint implants. *Clin Orthop Relat Res.* 2015;473:760–6.
18. Fu J, Shen J, Gao G, Xu Y, Hou R, Cong Y, Cheng Y. Natural polyphenol-stabilised highly crosslinked UHMWPE with high mechanical properties and low wear for joint implants. *J Mater Chem B.* 2013;1:4727–35.
19. Oral E, Ghali BW, Rowell SL, Micheli BR, Lozynsky AJ, Muratoglu OK. A surface crosslinked UHMWPE stabilized by vitamin E with low wear and high fatigue strength. *Biomater.* 2010;31:7051–60.
20. Souza VC, Fim FC, Lima ME, Silva LB. Antioxidant effects of vitamin C on biomedical UHMWPE compounds. *Macromol Symp.* 2019;383(1–10):1800002.
21. Kurtz SM, Bracco P, Costa L, Oral E, Muratoglu OK. Vitamin E-blended UHMWPE biomaterials. In: *UHMWPE biomaterials handbook*. Norwich: William Andrew Publishing; 2016. p. 293–306.
22. Trouillas P, Marsal P, Svobodová A, Vostalova J, Gažák R, Hrbac J, Sedmera P, Křen V, Lazzaroni R, Duroux JL, Walterova D. Mechanism of the antioxidant action of silybin and 2, 3-dehydrosilybin flavonolignans: a joint experimental and theoretical study. *J Phys Chem A.* 2008;112:1054–63.
23. Reina M, Martínez A. Is silybin the best free radical scavenger compound in silymarin? *J Phys Chem B.* 2016;120:4568–78.
24. Martínez A, Reina M. Copper or free radical scavenger?, *Comput. Theor Chem.* 2017;1104:1–11.
25. Van Mourik JH. Experiences with silica gel as adsorbent. *Am Ind Hyg Assoc J.* 1965;26:498–509.
26. Haines PJ. *Thermal methods of analysis: principles, applications and problems*. Dordrecht: Springer Science & Business Media; 1995.
27. Coats AW, Redfern JP. Kinetic parameters from thermogravimetric data. *Nature.* 1964;201:68–9.
28. Flynn JH, Wall LA. A quick, direct method for the determination of activation energy from thermogravimetric data. *J Polym Sci B: Polym Lett.* 1966;4:323–8.
29. Ozawa T. A new method of analyzing thermogravimetric data. *Bull Chem Soc Jpn.* 1965;38:1881–6.
30. Kissinger HE. Reaction kinetics in differential thermal analysis. *Anal Chem.* 1957;29:1702–6.
31. Akahira TJ, Sunose T. Method of determining activation deterioration constant of electrical insulating materials. *Res Rep Chiba Inst Technol.* 1971;16:22–31.
32. Starink MJ. The determination of activation energy from linear heating rate experiments: a comparison of the accuracy of isoconversion methods. *Thermochim Acta.* 2003;404:163–76.
33. Friedman HL. Kinetics of thermal degradation of char-forming plastics from thermogravimetry. Application to a phenolic plastic. *J Polym Sci Part C Polym Symp.* 1964;6:183–95.
34. Norwicz J, Hajduk N. The accuracy of equations approximating the temperature integral part I. *J Therm Anal.* 1978;13:223–30.
35. Hajduk N, Norwicz J. The accuracy of equations approximating the temperature integral. Part II. *J Therm Anal.* 1979;16:193–5.
36. Doyle CD. Kinetic analysis of thermogravimetric data. *J App Poly Sci.* 1961;5:285–92.
37. Doyle CD. Series approximations to the equation of thermogravimetric data. *Nature.* 1965;207:290–1.
38. Sharma P, Kaur T, Pandey OP. In situ single-step reduction and silicidation of  $\text{MoO}_3$  to form  $\text{MoSi}_2$ . *J Am Ceram.* 2019;102:1522–34.
39. Georgieva V, Vezdova D, Vlaev L. Non-isothermal kinetics of thermal degradation of chitin. *J Therm Anal Calorim.* 2013;111:763–71.
40. Sharma P, Pandey OP, Diwan PK. Non-isothermal kinetics of pseudo-components of waste biomass. *Fuel.* 2019;253:1149–61.
41. Çilgi GK, Ak M. Thermal degradation kinetics and thermodynamics of maleimide-styrene based alternating copolymer: a comparative investigation of monomer and polymer structures. *J Mol Str.* 2020;1221:128879.
42. Kirschweng B, Vörös B, Tátraaljai D, Zsuga M, Földes E, Pukánszky B. Natural antioxidants as melt stabilizers for PE: comparison of silymarin and quercetin. *Eur Polym J.* 2017;90:456–66.
43. Kirschweng B, Tátraaljai D, Földes E, Pukánszky B. Natural antioxidants as stabilizers for polymers. *Polym Degrad Stab.* 2017;145:25–40.
44. Chen F, Chi C. Development of pullulan/carboxylated cellulose nanocrystal/tea polyphenol bio nanocomposite films for active food packaging. *Int J Biol Macromol.* 2021;186:405–13.
45. Souza VC, Oliveira JE, Lima SJ, Silva LB. Influence of vitamin C on morphological and thermal behaviour of biomedical UHMWPE. *Macromol Symp.* 2014;344:8–13.
46. Padrón AJ, Colmenares MA, Rubinstain Z, Alborno LA. Influence of additives on some physical properties of high density polyethylene-I. Commercial antioxidants. *Eur Polym J.* 1987;23:723–7.
47. Xu J, Reiter G, Alamo RG. Concepts of nucleation in polymer crystallization. *Crystals.* 2021;11:304.

**Publisher's Note** Springer Nature remains neutral with regard to jurisdictional claims in published maps and institutional affiliations.